

Damping of dynamical friction force in self-interacting ultralight dark matter and Fornax timing problem

E.V. Gorbar^{1,2}, O.V. Barabash¹, V.M. Gorkavenko^{1,2}, K. Korshynska^{3,4},
A.I. Momot¹, A.O. Zaporozhchenko¹

¹ *Faculty of Physics, Taras Shevchenko National University of Kyiv,
64, Volodymyrs'ka str., Kyiv 01601, Ukraine*

² *Bogolyubov Institute for Theoretical Physics, National Academy of Sciences of Ukraine,
14-b, Metrolohichna str., Kyiv 03143, Ukraine*

³ *Institut für Mathematische Physik, Technische Universität Braunschweig,
Mendelssohnstraße 3, 38106 Braunschweig, Germany*

⁴ *Fundamentale Physik für Metrologie FPM, Physikalisch-Technische Bundesanstalt PTB,
Bundesallee 100, 38116 Braunschweig, Germany*

Abstract

The dynamics of globular clusters in the Fornax dwarf galaxy poses a challenge for the standard cold dark matter and can be used to test other models of dark matter. We study this dynamics in the context of ultralight bosonic dark matter model, accounting for the damping term in a generalized Gross-Pitaevskii equation. Employing analytic formulas for the dynamical friction force, the infall time and evolution of globular clusters are compared in the cases with and without the damping term. It is argued that the damping term plays an important role for the Fornax timing problem in ultralight dark matter (ULDM) models. In particular, the infall time of globular cluster GC3 can attain the required value, provided that ULDM is non-interacting or has a very small repulsive self-interaction. In the strongly-interacting ULDM, there is no solution for the required infall time for GC3 if its starting position is $r_0 \lesssim 1.5$ kpc.

Keywords: ultralight dark matter, Fornax dwarf galaxy, globular clusters, dynamical friction force

1 Introduction

Globular clusters are large and dense agglomerates of stars with typical half-light radius 3-5 pc up to tens of pc with masses $10^3 M_\odot - 10^6 M_\odot$ [1]. For example, it is estimated that the Milky Way contains more than 150 globular clusters with majority of them in the Milky Way halo. Globular clusters are observed also in dwarf galaxies, which typically orbit or interact with larger more massive galaxies like the Milky Way.

It was argued a long time ago that the dynamical friction can strongly affect the orbits of globular clusters [2]. One of the most studied cases is the Fornax dwarf spheroidal, which is a satellite of the Milky Way and contains six globular clusters (GC) [3]. The

orbital decay timescale for these globular clusters to sink toward the galactic nucleus due to dynamical friction is ~ 1 Gyr in the cold dark matter (CDM) model [4], which is much less than the Hubble time. It is worth mentioning also that this Fornax timing problem [5] was revisited in [6] via N-body simulations, where it was concluded that dismissing the presence of a cusp in Fornax based on the spatial distribution of its GC population is unwarranted. Globular clusters were studied too in other dwarf galaxies. For example, recent study in [7] showed that the observed distribution of globular clusters in ultra-diffusive NGC5846-UDG1 harbouring around 59 globular clusters is indicative of their mass segregation induced by dynamical friction.

One possible resolution to the Fornax globular cluster problem is the proposition that the dark matter halo in Fornax is cored [5, 8–10] with the core size of $r_c \geq 0.5$ kpc [11]. Then the Fornax timing problem is resolved due to ‘dynamical buoyancy’ created by the core. Dark matter distribution in massive and dwarf galaxies is naturally cored in models of dark matter composed of ultralight bosons with typical value of mass 10^{-22} eV, where core is formed by the Bose-Einstein condensate (BEC) of ultralight bosons (for a review, see [12, 13]). Models of ultralight dark matter (ULDM) have quite interesting phenomenology and are actively studied in the literature because while they could reproduce the large-scale structure of the Universe successfully explained in cold dark matter models, ULDM models are free of some problems which CDM models encounter at galactic scale. In addition, the ULDM self-interaction could also critically impact the dynamics and distribution of globular clusters in ultra-diffuse galaxies, leading to their segregation by mass [14].

Further, dark matter halos in ultralight dark matter models have a nontrivial structure and consist of a solitonic core and an isothermal atmosphere [15, 16]. The corresponding generalized Gross-Pitaevskii equation, which describes these halos, contains a logarithmic nonlinearity associated with a nonzero temperature and a source of dissipation. Employing the Madelung transformation, it is found [15] that the latter enters the hydrodynamic equations as a damping term linear in hydrodynamic velocity. Euristicly, the presence of such a term could lead to the dissipation of perturbations in ultralight dark matter produced by a moving object and decrease the dynamical friction force, thus, alleviating the timing problem of Fornax globular clusters.

The orbital decay timescale for the Fornax globular clusters to sink toward the galactic nucleus due to dynamical friction was considered, e.g., in [17, 18] in different models of dark matter (DM). It was concluded that infall time could be greater than 10 Gyr for all globular clusters except GC3. The case of globular cluster GC3 is the most problematic because GC3 is considered to be formed in situ and has an estimated age of approximately 12 Gyr [19, 20].

Euristic considerations mentioned above motivate us to study in this paper the impact of the damping term on the dynamical friction force acting on globular clusters moving in self-interacting ULDM environment and check whether it could help to resolve the Fornax timing problem, especially for the GC3 globular cluster.

The paper is organized as follows. The model used in our study is described in Sec. 2. The dynamical friction force acting on moving globular clusters is considered in Sec. 3. In Sec. 4 the ultralight dark matter density in Fornax dwarf is described. In Sec. 5 we compute the dynamical friction force in the Fornax dwarf galaxy. Numerical results for the trajectory and infall time of moving globular clusters in the Fornax dwarf galaxy are given in Sec. 6. Conclusions are drawn in Sec. 7.

2 Model

Let us begin our analysis by writing down the generalized Gross-Pitaevskii-Poisson equation [15] which governs the dynamical evolution of self-gravitating and self-interacting BEC field ψ

$$i\hbar\frac{\partial\psi}{\partial t} = \left(-\frac{\hbar^2}{2m}\nabla^2 + m\Phi_g + gN|\psi|^2 + 2k_B T \ln|\psi|\psi - \frac{i\hbar\xi}{2} \left[\ln\left(\frac{\psi}{\psi^*}\right) - \ln\left(\frac{\psi^*}{\psi}\right) \right] \right) \psi, \quad (1)$$

where $g = 4\pi\hbar^2 a_s/m$ is the coupling strength of the self-interaction of dark matter particles with mass m , and the s -wave scattering length a_s . Here N is the number of boson particles, and \hbar is the Planck constant. The first term on the right-hand side of the Gross-Pitaevskii equation (1) corresponds to the kinetic energy. Repulsive self-interaction is described by the nonlinear term in Eq. (1) with $g > 0$. The fourth term accounts for an isothermal halo with an effective temperature T surrounding the core. The last term is a damping term which ensures that the system relaxes to equilibrium, and its effect on the dynamical friction force is of principal interest to us in this study. The value of ξ was estimated in [15] via a generalized Einstein relation that expresses the fluctuation-dissipation theorem

$$\xi = \frac{2k_B T}{\hbar}, \quad (2)$$

where k_B is the Boltzmann constant.

The second term in the generalized Gross-Pitaevskii equation (1) contains the self-consistent gravitational potential Φ_g , which supports the formation of a localized BEC core and is defined by the Poisson equation

$$\nabla^2\Phi_g = 4\pi GmN|\psi|^2, \quad (3)$$

where G is the gravitational constant.

In our derivation of the dynamical friction force, we follow the setup developed in Refs. [21,22] where the dynamical friction force was given as double sum over the azimuthal and quantum numbers (for extension to the case of a Plummer sphere moving on a circular orbit, see Refs. [23,24]) and generalize it to the case of nonzero ξ . An orbiting object (star, globular cluster, dwarf galaxy, etc.) moving in a homogeneous ultralight dark matter composed of ultralight bosonic particles of mass m perturbs the ULDM density $\rho(t, \mathbf{r}) = \rho_{\text{DM}}(1 + \alpha(t, \mathbf{r}))$ due to gravitational interaction. In the linear response approach, we find that the corresponding density inhomogeneity $\alpha(t, \mathbf{r})$ is governed by the equation

$$\partial_t^2\alpha - c_s^2\nabla_{\mathbf{r}}^2\alpha + \frac{\nabla_{\mathbf{r}}^4\alpha}{4m^2} + \xi\partial_t\alpha = 4\pi Gn(\mathbf{r} - \mathbf{r}_0(t)), \quad (4)$$

where $\mathbf{r}_0(t)$ denotes the position of the center of mass of the moving object and $n(\mathbf{r})$ is its mass density. In our study, we consider the case of a point perturber where $n(\mathbf{r}) = M\delta^3(\mathbf{r})$ with object's mass M . Here c_s is the sound velocity expressed through the ULDM pressure P via the standard formula $c_s^2 = \partial P/\partial\rho_{\text{DM}}$. In our case, the ULDM pressure is given by $P = \rho_{\text{DM}}^2 g/(2m^2) + \rho_{\text{DM}}k_B T/m$ [15] and therefore

$$c_s = \sqrt{\frac{\rho_{\text{DM}}g}{m^2} + \frac{k_B T}{m}}. \quad (5)$$

In momentum space, we have Eq.(4) for steady-state motion gives

$$\alpha(\omega, \mathbf{k}) = 4\pi GM \int_{-\infty}^{+\infty} dt' \frac{e^{i\omega t' - i\mathbf{k}\mathbf{r}_0(t')}}{-\omega^2 + c_s^2 k^2 + \frac{k^4}{4m^2} - i\xi\omega}. \quad (6)$$

According to the Poisson equation, the density inhomogeneity $\alpha(t, \mathbf{r})$ and the moving object source a perturbation $\phi(t, \mathbf{r})$ of the gravitational potential

$$\nabla^2 \phi(t, \mathbf{r}) = 4\pi G(\rho_{\text{DM}} \alpha(t, \mathbf{r}) + M\delta^3(\mathbf{r} - \mathbf{r}_0(t))). \quad (7)$$

Eq. (7) gives the following gravitational potential due to perturbed ULDM density (the complete perturbed gravitational potential is obviously the sum $\phi = \phi_\alpha + \phi_0$, where ϕ_0 is the Newtonian potential of the moving perturber):

$$\phi_\alpha(t, \mathbf{r}) = -4\pi G\rho_{\text{DM}} \int \frac{d\omega d\mathbf{k}}{(2\pi)^4} \frac{\alpha(\omega, \mathbf{k})}{k^2} e^{-i\omega t + i\mathbf{k}\mathbf{r}}, \quad (8)$$

where $\alpha(\omega, \mathbf{k})$ is given by (6) and ρ_{DM} can be approximated to be a constant in view of the hierarchy of masses of the Milky Way and perturber.

3 Dynamical friction force with damping term

Using the obtained gravitational potential of perturbed dark matter due to the moving perturber, we easily find the dynamical friction force

$$\mathbf{F}_{\text{fr}}(t) = -M\nabla_{\mathbf{r}}\phi_\alpha(t, \mathbf{r})|_{\mathbf{r}=\mathbf{r}_0(t)} = 4\pi G\rho_{\text{DM}}M \int \frac{d\omega d\mathbf{k}}{(2\pi)^4} \frac{i\mathbf{k}}{k^2} \alpha(\omega, \mathbf{k}) e^{-i\omega t + i\mathbf{k}\mathbf{r}_0(t)}. \quad (9)$$

It is convenient to change the variable $\tau = t - t'$ and then take into account that the integral over ω vanishes for $\tau < 0$. Finally, taking into account Eq. (6), we get the dynamical friction force

$$\mathbf{F}_{\text{fr}}(t) = \frac{G^2 M^2 \rho_{\text{DM}}}{\pi^2} \int_0^{+\infty} d\tau \int d\omega d\mathbf{k} \frac{i\mathbf{k}}{k^2} \frac{e^{-i\omega\tau + i\mathbf{k}\mathbf{r}_0(t) - i\mathbf{k}\mathbf{r}_0(t-\tau)}}{-\omega^2 - i\xi\omega + c_s^2 k^2 + \frac{k^4}{4m^2}}. \quad (10)$$

It is important to note that if the damping term is absent, then the same expression for the dynamical term applies with the replacement $\xi \rightarrow \delta$ where $\delta \rightarrow +0$ reproducing the dynamical friction force obtained in [25].

The poles of the integrand in Eq. (10) are given by

$$\omega_{1,2} = -\frac{i\xi}{2} \pm D(k), \quad D(k) = \sqrt{-\frac{\xi^2}{4} + c_s^2 k^2 + \frac{k^4}{4m^2}}. \quad (11)$$

Since they are always located in the lower half-plane of the complex plane ω , we should close the contour over ω in the lower half-plane for $\tau > 0$. Integration over ω in Eq. (10) yields

$$\mathbf{F}_{\text{fr}}(t) = \frac{2G^2 M^2 \rho_{\text{DM}}}{\pi} \int_0^{+\infty} d\tau \int d\mathbf{k} \frac{i\mathbf{k}}{k^2 D(k)} e^{i\mathbf{k}\mathbf{r}_0(t) - i\mathbf{k}\mathbf{r}_0(t-\tau)} e^{-\xi\tau/2} \sin(\tau D(k)). \quad (12)$$

Assuming that GC rotates on a circular orbit with angular velocity Ω directed along the z -axis, we have

$$\mathbf{r}_0(t) = r_0(\cos(\Omega t), \sin(\Omega t), 0), \quad \mathbf{k} = (\mathbf{k}_p, k_z), \quad \mathbf{k}_p = (k_p \cos \phi, k_p \sin \phi)$$

and

$$\mathbf{k}\mathbf{r}_0(t) - \mathbf{k}\mathbf{r}_0(t - \tau) = k_p r_0 \left(\cos(\Omega t - \phi) - \cos(\Omega(t - \tau) - \phi) \right),$$

where r_0 is the orbit radius.

Setting without loss of generality $t = 0$, we obtain

$$\mathbf{F}_{\text{fr}} = \frac{2G^2 M^2 \rho_{\text{DM}}}{\pi} \int_0^{+\infty} d\tau \int_{-\infty}^{+\infty} dk_z \int_0^{\infty} k_p dk_p \int_0^{2\pi} d\phi \frac{i\mathbf{k}}{k^2 D(k)} e^{ik_p r_0 (\cos \phi - \cos(\phi + \Omega\tau))} e^{-\xi\tau/2} \sin(\tau D(k)). \quad (13)$$

Obviously, the z -component of this force vanishes because the integrand is odd in k_z .

We can split the integral over ϕ in Eq. (13) into two integrals, $\int_0^{2\pi} = \int_0^{\pi} + \int_{\pi}^{2\pi}$, and make the change of variable $\phi' = \phi - \pi$ in the second

$$I_\phi = \int_0^{2\pi} d\phi \mathbf{k}_p(\phi) e^{if(\phi)} = \int_0^{\pi} d\phi \mathbf{k}_p(\phi) e^{if(\phi)} + \int_0^{\pi} d\phi' \mathbf{k}_p(\phi' + \pi) e^{if(\phi' + \pi)}, \quad (14)$$

where $f(\phi) = k_p r_0 (\cos \phi - \cos(\phi + \Omega\tau))$ and $\mathbf{k}_p(\phi) = (k_p \cos \phi, k_p \sin \phi)$, hence $f(\phi' + \pi) = -f(\phi')$ and $\mathbf{k}_p(\phi' + \pi) = -\mathbf{k}_p(\phi')$. Thus, we get

$$I_\phi = \int_0^{\pi} d\phi \mathbf{k}_p(\phi) (e^{if(\phi)} - e^{-if(\phi)}) = 2i \int_0^{\pi} d\phi \mathbf{k}_p(\phi) \sin(f(\phi)). \quad (15)$$

Using the obtained relation, we can express the dynamical friction force in the explicitly real form

$$\mathbf{F}_{\text{fr}} = F_r \hat{\mathbf{r}} + F_t \hat{\boldsymbol{\phi}} = -\frac{4G^2 M^2 \rho_{\text{DM}}}{\pi} \int_0^{+\infty} d\tau \int_{-\infty}^{+\infty} dk_z \int_0^{\infty} k_p dk_p \int_0^{\pi} d\phi \frac{\hat{\mathbf{r}} k_p \cos \phi + \hat{\boldsymbol{\phi}} k_p \sin \phi}{k^2 D(k)} \times \sin [k_p r_0 (\cos \phi - \cos(\phi + \Omega\tau))] e^{-\xi\tau/2} \sin(\tau D(k)), \quad (16)$$

where F_r and F_t are the tangential and radial components of the dynamical friction force.

4 DM density in Fornax dwarf galaxy

In what follows, we use the properties of DM halo of Fornax inferred from observations in [26], where the Fornax mass was modeled to be $M = 5.8_{-0.2}^{+1} \cdot 10^7 M_\odot$ as the best fit of the observations of stellar light profile and stellar kinematics. The authors also found that the DM halo density has to be approximately constant and of the order of $\rho_{\text{obs}} = (1.6 \pm 0.1) \cdot 10^{-2} M_\odot \cdot \text{pc}^{-3}$. This observation thus disfavors a cuspy CDM density in the center and suggests the presence of a core, which is one of the prominent features of

ULDM. For our analysis, we adopt the value of the density $\rho(r_h) = \rho_{\text{obs}}$, where $r_h \approx 710$ pc is the observed half-light radius of the Fornax halo [27], which, in what follows, is referred to as the halo radius.

Note that for a known density profile $\rho(r)$, one can easily derive the corresponding rotation velocity of a test particle (e.g., star) in the gravitational potential produced by $\rho(r)$ [28]

$$v(r) = [GM(r)/r]^{1/2}, \quad M(r) = 4\pi \int_0^r dr' (r')^2 \rho(r'), \quad (17)$$

where $M(r)$ is the total ULDM mass within the radius r .

Having discussed the properties of the dark matter halo, we can now proceed to its description using ULDM models. A particular ULDM model is fixed when a specific boson candidate with mass m and the s-wave scattering length a_s is considered. Then, for given $\{m, a_s\}$, the ULDM halo density $\rho(r)$ can be found as a solution to Eq. (1). The density profile of this solution is dominated by the inner fully coherent core with slowly varying density [15]. In the core region, the effective temperature term $\sim k_B T$ in Eq. (1) is small compared to the other terms and can be neglected [15], so that the core can be well-approximated by a solution to the ordinary GPP equations without dissipation. Beyond the core the effective temperature term dominates in the generalized GPP equation and gives rise to a dilute isothermal envelope. Thus, following the analysis in [15], we consider the approximate analytical expressions for the ULDM density $\rho(r)$ in these two regions separately.

We first focus on the central region of the ULDM halo, which is described by a BEC soliton solution of GPP equations [15, 28]. Its shape is determined by dimensionless parameter χ [28]

$$\chi = \frac{GM^2 m a_s}{\hbar^2}, \quad (18)$$

which sets the boundary between the Gaussian and Thomas-Fermi (TF) approximation regimes. The Gaussian ansatz approximates best the soliton density in the absence of short-range interactions ($a_s = 0$) and is valid only for small and moderate values of $\chi \lesssim 1$. In the other regime of $\chi \gg 1$, the repulsive interactions play a dominant role in counteracting gravitational attraction, leading to a TF density profile. While these density profiles will be discussed further in Secs. 4.1-4.2, we find that for Fornax

$$\chi = 1.42 \cdot 10^{83} \frac{a_s}{\text{fm}} \frac{m}{\text{eV}}, \quad (19)$$

where fm = 10^{-15} meters. This means that for a boson mass $\sim 10^{-22}$ eV, a characteristic value of the s-wave scattering length is of order 10^{-76} meters and decreases for larger boson masses.

4.1 Thomas-Fermi density: strong repulsive interaction

If the DM particle has a strong repulsive interaction, the TF approximation is applicable. In this approximation, the ground state density of the soliton reads

$$\rho_{\text{TF}}(r) = \rho_0^{\text{TF}} \frac{\sin(\pi r/R_{\text{TF}})}{\pi r/R_{\text{TF}}}, \quad \rho_0^{\text{TF}} = \frac{\pi M}{4R_{\text{TF}}^3} \quad (20)$$

and lies compactly within $r \in [0, R_{\text{TF}}]$. Fitting $\rho_{\text{TF}}(r_h) = \rho_{\text{obs}}$ fixes $R_{\text{TF}} = 1$ kpc and $\rho_0^{\text{TF}} = 4.56 \cdot 10^{-2} M_{\odot}/\text{pc}^3$. Using the density profile (20), we can infer the properties of the ULDM. The TF radius is related to the ULDM parameters $\{m, a_s\}$ via

$$R_{\text{TF}} = \pi \left(\frac{a_s \hbar^2}{Gm^3} \right)^{1/2} \quad (21)$$

as shown in [29]. This implies that

$$\frac{a_s}{\text{fm}} \left(\frac{\text{eV}/c^2}{m} \right)^3 = 3.28 \cdot 10^3, \quad (22)$$

which is the same constraint as found in [15]. In fact, this relation links the s -wave scattering length a_s (or the coupling strength of the self-interaction $g = 4\pi\hbar^2 a_s/m$) and the mass m of a dark matter particle. Plugging this relation into (19), we obtain $m \gg 2.15 \cdot 10^{-22}$ eV. Therefore, we conclude that for boson masses $m > 10^{-21}$ eV, the ULDM density profile can be approximated by the TF density (20).

For the analytically found TF density distribution (20), one can infer the rotation curve [15]

$$v^2(r) = \frac{4G\rho_0 R_{\text{TF}}^2}{\pi} \left[\frac{R_{\text{TF}}}{\pi r} \sin\left(\frac{\pi r}{R_{\text{TF}}}\right) - \cos\left(\frac{\pi r}{R_{\text{TF}}}\right) \right], \quad (23)$$

$$\frac{v(r)}{\text{km/s}} = 15.8 \left[\frac{318.3 \text{ pc}}{r} \sin\left(\frac{r}{318.3 \text{ pc}}\right) - \cos\left(\frac{r}{318.3 \text{ pc}}\right) \right]^{1/2}, \quad (24)$$

where the latter formula is given for the parameters of the Fornax ULDM halo defined above.

4.2 Gaussian density: weak interaction

In the case of non-interacting BEC or moderate interaction strength, one can approximate the ULDM density profile by the Gaussian ansatz [28], which reads

$$\rho_G(r) = \rho_0^G e^{-r^2/R^2}, \quad \rho_0^G = \frac{M}{\pi^{3/2} R^3}. \quad (25)$$

The condition $\rho_{\text{obs}} = \rho_G(r_h)$ is best satisfied by the choice $R = 581$ pc in Eq. (25) giving the central density $\rho_0^G = 5.31 \cdot 10^{-2} M_{\odot}/\text{pc}^3$. We can again deduce the ultralight boson properties from the fixed ULDM halo properties. Imposing the condition that the soliton energy must be minimized, one can find the corresponding mass-radius relation [13, 28, 30, 31]

$$R = \frac{\sigma}{\nu} \frac{\hbar^2}{GMm^2} \left(1 \pm \sqrt{1 + \frac{6\pi\zeta\nu GmM^2 a_s}{\sigma^2 \hbar^2}} \right), \quad (26)$$

where $\sigma = 3/4$, $\nu = 1/\sqrt{2\pi}$, and $\zeta = 1/(2\pi)^{3/2}$. The sign '+' stands for the case of repulsive or no self-interaction $a_s \geq 0$, while the sign ' \pm ' represents the case of attractive self-interaction $a_s < 0$. In what follows, we focus on the $a_s \geq 0$ regime. Plugging the known parameters M and R into this relation, we obtain the dependence of the s -wave

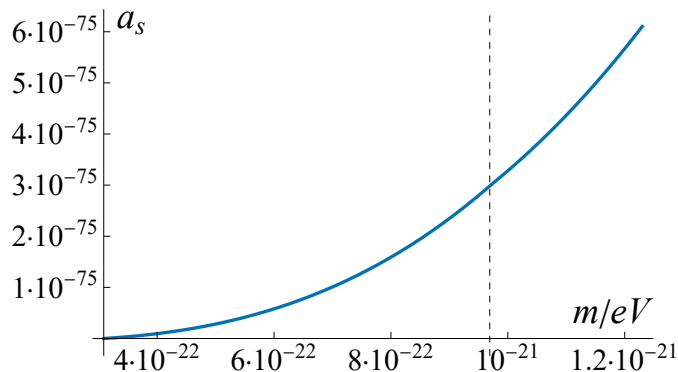


Figure 1: The dependence of s -wave scattering length a_s (in meters) on the mass of the ULDM particle m defined by Eq. (22) for $m > 10^{-21}$ eV and Eq. (27) for $m < 10^{-21}$ eV. The dashed vertical line separates the Gaussian density (left) from the TF (right) density approximation.

scattering length a_s (or the coupling strength of the self-interaction $g = 4\pi\hbar^2 a_s/m$) on mass of the DM particle

$$\left(\frac{m}{\text{eV}/c^2}\right)^2 = 4.76 \cdot 10^{-44} \left(1 + \sqrt{1 + 1.21 \cdot 10^{83} \frac{a_s}{\text{fm}} \frac{m}{\text{eV}}}\right) \quad (27)$$

that can be written in the form

$$\frac{a_s}{\text{fm}} = -3.47 \cdot 10^{-40} \frac{m}{\text{eV}} + 3.65 \cdot 10^3 \left(\frac{m}{\text{eV}}\right)^3. \quad (28)$$

As one can see, in the non-interacting case $a_s = 0$, the above relation gives the boson mass $m = 3.09 \cdot 10^{-22}$ eV. For larger masses m , ULDM self-interaction is attractive. The dependence of the s -wave scattering length a_s on the mass of the DM particle m is presented in Fig.1.

For the analytically determined Gaussian density (25), one can derive the rotation curve [32]

$$v^2(r) = \frac{GM}{R} \left[\frac{R}{r} \text{erf}\left(\frac{r}{R}\right) - \frac{2}{\sqrt{\pi}} e^{-(r/R)^2} \right], \quad (29)$$

$$\frac{v(r)}{1\text{km/s}} = 20.7 \left[\frac{581 \text{ pc}}{r} \text{erf}\left(\frac{r}{581 \text{ pc}}\right) - \frac{2}{\sqrt{\pi}} \exp\left[-\left(\frac{r}{581 \text{ pc}}\right)^2\right] \right]^{1/2}. \quad (30)$$

4.3 Full ULDM halo with core and envelope

Having described a compact soliton core in the central region, we now discuss the isothermal envelope on the outskirts of the ULDM halo. Its density has the shape of the Navarro-Frenk-White (NFW) density profile [33], which is given by

$$\rho_{\text{NFW}}(r) = \frac{\rho_e}{r/r_e(1+r/r_e)^2}, \quad (31)$$

while the gravitational potential and the mass enclosed within the radius r read

$$\Phi_{\text{NFW}}(r) = -\frac{4\pi G\rho_e r_e^3}{r} \ln\left(1 + \frac{r}{r_e}\right), \quad (32)$$

$$M_{\text{NFW}}(r) = 4\pi \int_0^r \rho(x)x^2 dx = 4\pi\rho_e r_e^3 \left[\ln\left(1 + \frac{r}{r_e}\right) - \frac{r/r_e}{1 + r/r_e} \right]. \quad (33)$$

To construct a realistic model of the Fornax dark matter halo, we need to account for the observations of the stellar velocity dispersion σ_v . The theory prediction can be found using [34]

$$\overline{v^2} = \frac{1}{\rho_{\text{NFW}}(r)} \int_r^\infty dr' \rho_{\text{NFW}}(r') \frac{d\Phi_{\text{NFW}}}{dr'} \approx -\frac{\pi}{4} G\rho_e r_e^2 \frac{r_e}{r} \left[3 + 4 \ln\left(\frac{r_e}{r}\right) \right], \quad (34)$$

where the last expression is given for $r_e/r \ll 1$ (far from the halo center). Thus, we find the velocity dispersion to be

$$\sigma_v = (\overline{v^2})^{1/2} = \sqrt{G\rho_e r_e^2} \sqrt{-\frac{\pi}{4} \frac{r_e}{r} \left[3 + 4 \ln\left(\frac{r_e}{r}\right) \right]}, \quad (35)$$

which is a slowly decaying function of r . On the outskirts of the BEC core, at distance $r = 1$ kpc (this is the TF radius R_{TF} as found in Sec. 4.1), according to the observations [35], the velocity dispersion of Fornax is $\sigma_v = 8$ km/s. At this distance Eq. (35) gives $\sigma_v = 0.32\sqrt{G\rho_e r_e^2}$, where we used $r_e \approx 8$ pc (the exact value of r_e will be determined in what follows). Then, we obtain the relation

$$\rho_e r_e^2 = \frac{625 \text{ km}^2/\text{s}^2}{G} = 1.45 \cdot 10^5 M_\odot/\text{pc} = \kappa \quad (36)$$

for parameters ρ_e and r_e characterizing the NFW envelope (31).

4.4 Soliton radius and continuous transition between soliton and envelope

Following Ref. [20], we match the core (soliton) and envelope densities at a certain radial distance r_t by fixing the corresponding densities $\rho_{\text{NFW}}(r_t) = \rho_s(r_t)$ and masses enclosed within radius r_t , namely, $M_{\text{NFW}}(r_t) = M_s(r_t)$.

If we model the soliton using the Gaussian density, see Sec. 4.2, with

$$\rho_G(r) = \rho_0^G e^{-r^2/R^2}, \quad (37)$$

$$M_s(r) = \pi\rho_0^G R^2 \left[-2re^{-r^2/R^2} + \sqrt{\pi}R \operatorname{erf}\left(\frac{r}{R}\right) \right], \quad (38)$$

then the two continuity conditions at $r = r_t$ read

$$\begin{aligned} \rho_e \frac{1}{r_t/r_e(1 + r_t/r_e)^2} &= \rho_0^G e^{-r_t^2/R^2}, \\ 4\pi\rho_e r_e^3 \left[\ln\left(1 + \frac{r_t}{r_e}\right) - \frac{r_t/r_e}{1 + r_t/r_e} \right] &= \pi\rho_0^G R^2 \left[-2r_t e^{-r_t^2/R^2} + \sqrt{\pi}R \operatorname{erf}\left(\frac{r_t}{R}\right) \right]. \end{aligned}$$

Note that parameters $\rho_0^G = 5.31 \cdot 10^{-2} M_\odot/\text{pc}^3$ and $R = 581 \text{ pc}$ are known, see Sec. 4.2, and $\rho_e = \kappa/r_e^2$ is derived from the observations of velocity dispersion, see Eq. (36). Thus, the only unknown parameters are r_e and r_t which should be determined from the equations above.

For simplicity, we measure all masses in units of M_\odot and all distances in units of kpc. Then we have the equations

$$\begin{aligned} 2.735 \frac{1}{r_e^2} \frac{1}{r_t/r_e(1+r_t/r_e)^2} &= e^{-r_t^2/0.581^2}, \\ 10.94 r_e \left[\ln \left(1 + \frac{r_t}{r_e} \right) - \frac{r_t/r_e}{1+r_t/r_e} \right] &= 0.581^3 \left[-3.442 r_t e^{-r_t^2/0.581^2} + \sqrt{\pi} \operatorname{erf} \left(\frac{r_t}{0.581} \right) \right], \end{aligned}$$

giving $r_t = 1.238 \text{ kpc}$ and $r_e = r_t/165$. Thus, the transition between the core and envelope in this case occurs at distance r_t , where the density of both NFW and Gaussian soliton profiles equals $\rho(r_t) = 5.7 \cdot 10^{-4} M_\odot/\text{pc}^3$. Finally, for $3.09 \cdot 10^{-22} \text{ eV} < m < 10^{-21} \text{ eV}$, we can write down the overall density of DM as

$$\rho_{\text{DM}}(r) = \begin{cases} \rho_0^G e^{-r^2/R^2}, & r \leq r_t \\ \rho_e \frac{1}{r/r_e(1+r/r_e)^2}, & r > r_t, \end{cases} \quad (39)$$

where $\rho_0^G = 5.31 \cdot 10^{-2} M_\odot/\text{pc}^3$, $\rho_e = 2.59 \cdot 10^3 M_\odot/\text{pc}^3$, $r_t = 1238 \text{ pc}$, $R = 581 \text{ pc}$, and $r_e = 7.50 \text{ pc}$.

For the mass of dark matter particles $m > 10^{-21} \text{ eV}$, the repulsive interaction is strong and the soliton should be modeled using the Thomas-Fermi model, see Sec. 4.1, with the density

$$\rho_{\text{TF}}(r) = \rho_0^{\text{TF}} \frac{\sin(\pi r/R_{\text{TF}})}{\pi r/R_{\text{TF}}}, \quad (40)$$

$$M_s(r) = M \left[\frac{1}{\pi} \sin \left(\frac{\pi r}{R_{\text{TF}}} \right) - \frac{r}{R_{\text{TF}}} \cos \left(\frac{\pi r}{R_{\text{TF}}} \right) \right]. \quad (41)$$

Thus, at the transition radius $r = r_t$, we find the two continuity conditions

$$\begin{aligned} \rho_e \frac{1}{r_t/r_e(1+r_t/r_e)^2} &= \rho_0^{\text{TF}} \frac{\sin(\pi r_t/R_{\text{TF}})}{\pi r_t/R_{\text{TF}}}, \\ 4\pi \rho_e r_e^3 \left[\ln \left(1 + \frac{r_t}{r_e} \right) - \frac{r_t/r_e}{1+r_t/r_e} \right] &= M \left[\frac{1}{\pi} \sin \left(\frac{\pi r_t}{R_{\text{TF}}} \right) - \frac{r_t}{R_{\text{TF}}} \cos \left(\frac{\pi r_t}{R_{\text{TF}}} \right) \right]. \end{aligned}$$

Here, parameters $R_{\text{TF}} = 1 \text{ kpc}$ and $M = 5.8 \cdot 10^7 M_\odot$ are known and $\rho_e = \kappa/r_e^2$ (36). To find the unknown r_t and r_e , we reformulate the system of equations in dimensionless form, measuring masses in the units of M_\odot and distances in kpc

$$\begin{aligned} \frac{1}{r_e(1+r_t/r_e)^2} &= 0.3136 \frac{\sin(\pi r_t)}{\pi}, \\ r_e \left[\ln \left(1 + \frac{r_t}{r_e} \right) - \frac{r_t/r_e}{1+r_t/r_e} \right] &= 0.03177 \left[\frac{1}{\pi} \sin(\pi r_t) - r_t \cos(\pi r_t) \right], \end{aligned}$$

and find $r_e = 8.40 \text{ pc}$ and $r_t = 972.1 \text{ pc}$. This transition radius is close to the R_{TF} boundary of the soliton. Finally, for $m > 10^{-21} \text{ eV}$, we can write down the overall density

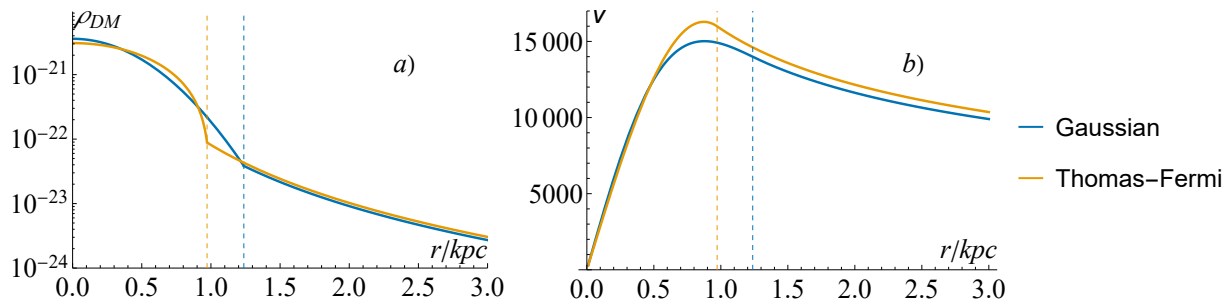


Figure 2: Panel *a*) Fornax mass density profiles ρ_{DM} (in kg/m^3). At the inflection points, the soliton dark matter density is stitched together with the NFW density profile. Panel *b*) Fornax rotation curves for the TF and Gaussian density distributions of ULDM soliton.

of ULDM as

$$\rho_{DM}(r) = \begin{cases} \rho_0^{\text{TF}} \frac{\sin(\pi r/R_{\text{TF}})}{\pi r/R_{\text{TF}}}, & r \leq r_t \\ \rho_e \frac{1}{r/r_e(1+r/r_e)^2}, & r > r_t, \end{cases} \quad (42)$$

where $\rho_0^{\text{TF}} = 0.0456 M_\odot/\text{pc}^3$, $\rho_e = 2.06 \cdot 10^3 M_\odot/\text{pc}^3$. The Fornax mass density profiles and rotation curves are presented in Fig.2.

5 Numerical results for dynamical friction in Fornax

To analyse numerically the obtained dynamical friction force, it is convenient to introduce the following dimensionless variables $K_z = k_z r_0$, $K_p = k_p r_0$, and $\mathcal{T} = \tau c_s / r_0$. In addition, $\mathcal{M} = r_0 \Omega / c_s$ is the Mach number, $A = m r_0 c_s$, and $\Xi = \xi r_0 / c_s$. Then

$$D(k) = \frac{\tilde{D}(K)}{2m r_0^2}, \quad \tilde{D}(K) = \sqrt{K^4 + 4A^2 K^2 - A^2 \Xi^2} \quad (43)$$

and the tangential component of the friction force (16) is

$$F_t = -\frac{4\pi G^2 M^2 \rho_{DM}}{c_s^2} \mathcal{F}_t, \quad (44)$$

where

$$\mathcal{F}_t = \frac{4A}{\pi^2} \int_0^{+\infty} d\mathcal{T} \int_0^{+\infty} dK_z \int_0^\infty K_p dK_p \int_0^\pi d\phi \frac{K_p \sin \phi}{K^2 \tilde{D}(k)} \\ \times \sin [K_p (\cos \phi - \cos(\phi + \mathcal{M}\mathcal{T}))] e^{-\Xi \mathcal{T}/2} \sin \left(\frac{\mathcal{T} \tilde{D}(k)}{2A} \right) \quad (45)$$

is the dimensionless tangential component of the dynamical friction force, where we used the fact that the integrand is an even function of k_z . In our numerical calculations, we replace the upper limits of integration in (45) with finite \mathcal{T}_{max} , $K_{z\text{max}}$, and $K_{p\text{max}}$ and then check that increasing these finite cut-offs does not affect the results.

It should be noted that ξ and the coupling strength of the self-interaction g are not independent parameters. The coupling strength of the self-interaction $g = 4\pi \hbar^2 a_s / m$ is determined by Eqs.(22) and (27). The dependence of the s-wave scattering length a_s on

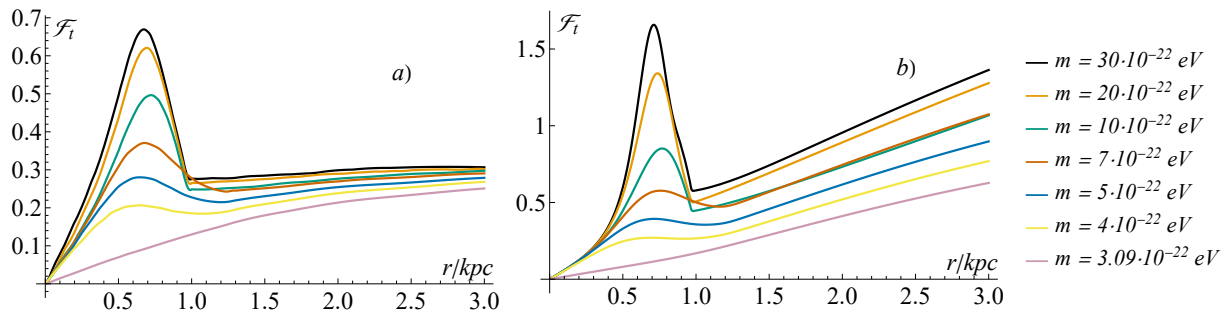


Figure 3: The tangential component of the dimensionless dynamical friction force \mathcal{F}_t as a function of distance from the Fornax dwarf galaxy center for several values of the ULDM boson mass: panel a) taking into account the damping term, panel b) neglecting the damping term ($\xi = 0$).

the mass of ULDM boson is shown in Fig. 1. While the value of ξ is defined by Eq. (2), the temperature of halo can be found from the condition [15]

$$k_B T = \frac{m \sigma_v^2}{2}, \quad (46)$$

where $\sigma_v = 8$ km/s is the stellar velocity dispersion for the Fornax dwarf galaxy [35].

Thus, we plot the tangential component of the dynamical friction force \mathcal{F}_t as a function of only two parameters: the mass of ULDM boson m and distance from the Fornax dwarf galaxy center, see Fig. 3. To compute the dynamical friction force for $m = 3.09 \cdot 10^{-22}$ eV, $4 \cdot 10^{-22}$ eV, $5 \cdot 10^{-22}$ eV, and $7 \cdot 10^{-22}$ eV, we used the Gaussian ansatz. For $m = 10^{-21}$ eV, $1.2 \cdot 10^{-21}$ eV, $2 \cdot 10^{-21}$ eV, and $2.7 \cdot 10^{-21}$ eV, the self-interaction is also repulsive and we use the Thomas-Fermi ansatz for the ULDM density. It should be noted that the lowest value of mass $m = 3.09 \cdot 10^{-22}$ eV is the minimum value for repulsive ULDM self-interaction, which corresponds to the absence of self-interaction. For smaller masses, the repulsive self-interaction turns into an attractive one.

According to Fig. 3, in general, \mathcal{F}_t increases as m grows, and a quite strong dependence on the boson mass m is observed for $r \leq 1$ kpc, resulting in a peak. The tangential component of the dynamical friction force attains a local maximum at $r \approx 0.6$ kpc. However, for larger distances, the behaviour of \mathcal{F}_t is different for the Gaussian and Thomas-Fermi regimes.

Comparing the results for the dynamical friction force in panels a) and b) of Fig. 3, one can see that taking into account the damping term essentially modifies (decreases) the magnitude of the dynamical friction force as well as change its behavior at large distances.

6 Trajectory and infall time of GC3

Having determined the dynamical friction force, we could now proceed to the evolution and motion of globular clusters. To describe them, we numerically solve the system of differential equations of motion

$$\begin{cases} m_{GC} \ddot{r} = -\frac{G m_{GC} M(r)}{r^2} + \frac{l^2}{m_{GC} r^3}, \\ \frac{dl}{dt} = -r(t) F_t(r), \end{cases} \quad (47)$$

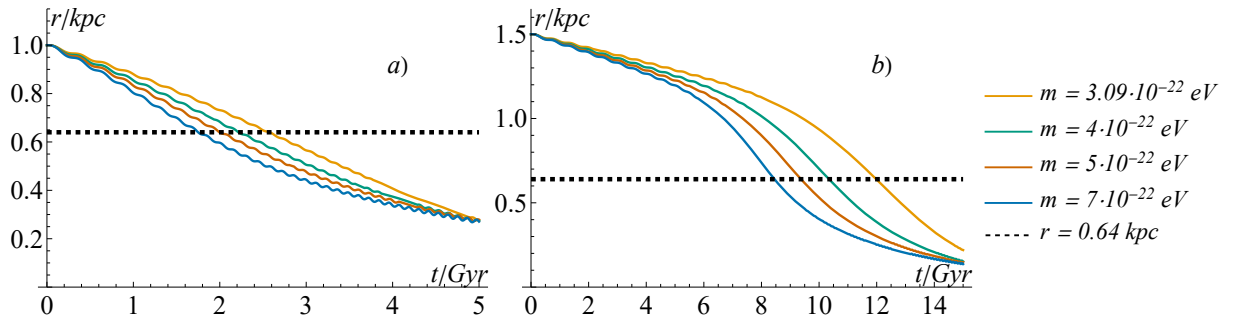


Figure 4: The trajectory $r(t)$ of the globular cluster GC3 as a function of time in the Gaussian regime and several values of the ULDM boson mass in the range $3.09 \cdot 10^{-22} \text{ eV} < m < 7 \cdot 10^{-22} \text{ eV}$ with its initial position panel *a*) $r_0 = 1 \text{ kpc}$ and panel *b*) $r_0 = 1.5 \text{ kpc}$. The black horizontal line indicates the current position of GC3.

where m_{GC} is the mass of GC, $l = m_{\text{GC}} r^2 \dot{\phi}$ is the angular momentum, see details in Appendix.

Setting the initial position of the globular cluster GC3 to be $r_0 = 1 \text{ kpc}$ and $r_0 = 1.5 \text{ kpc}$, zero initial value of its radial velocity, assuming its mass to be $m_{\text{GC}} = 4.98 \cdot 10^5 M_{\odot}$ [20], and solving the equations of motion (47), we plot the time dependence of $r(t)$ for the globular cluster GC3 in Fig.4 in the Gaussian regime (for several values in the range $3.09 \cdot 10^{-22} \text{ eV} < m < 7 \cdot 10^{-22} \text{ eV}$) and Thomas-Fermi regime Fig.5 (for several values in the range $10^{-21} \text{ eV} < m < 3 \cdot 10^{-21} \text{ eV}$). In both regimes, we see that the infall time decreases as mass m grows.

As one can see, in the Gaussian regime of weak repulsive self-interacting ULDM, which is valid for $3.09 \cdot 10^{-22} \text{ eV} < m \lesssim 10^{-21} \text{ eV}$, we cannot obtain the required time of 12 Gyr for GC3 to move from its assumed initial position $r_0 = 1 \text{ kpc}$ from the center of the Fornax galaxy to its current position at $r_{\text{GC3}} = 0.64 \text{ kpc}$ [20]. However, if we assume that GC3 was formed at larger distance, e.g., $r_0 = 1.5 \text{ kpc}$, where the density of dark matter and the force of dynamic friction are smaller, then it is possible to explain the observed lifetime of the cluster provided that $m \gtrsim 3.09 \cdot 10^{-22} \text{ eV}$. This value corresponds with $a_s = 0$ and sets the boundary between the regimes of repulsive and attractive self-interaction. This means that, for the initial position $r_0 = 1.5 \text{ kpc}$, the infall time of GC3 can be explained

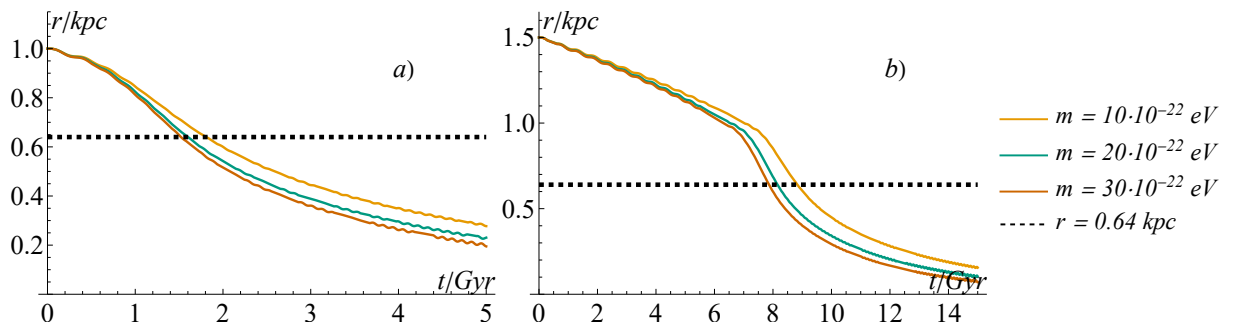


Figure 5: The trajectory $r(t)$ of the globular cluster GC3 as a function of time in the Thomas-Fermi regime for several values of the ULDM boson mass in the range $10^{-21} \text{ eV} < m < 3 \cdot 10^{-21} \text{ eV}$ with its initial position panel *a*) $r_0 = 1 \text{ kpc}$ and panel *b*) $r_0 = 1.5 \text{ kpc}$. The black horizontal line indicates the current position of GC3.

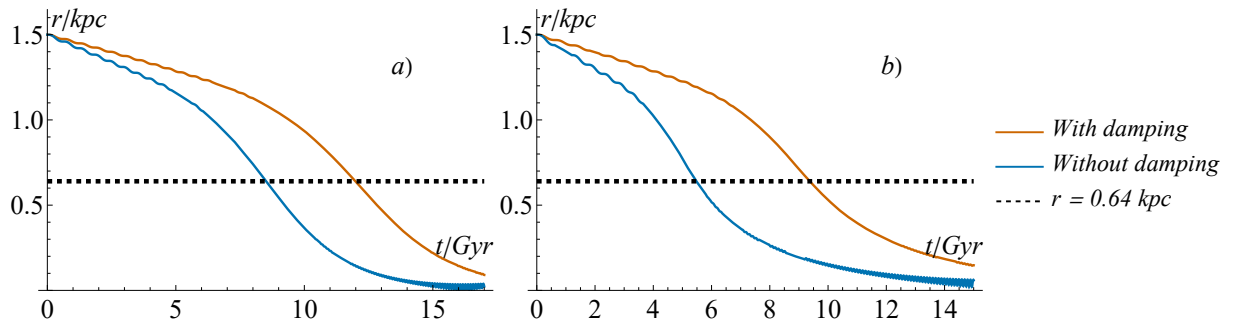


Figure 6: The trajectory $r(t)$ of the globular cluster GC3 as a function of time for several values of the ULDM boson mass $m = 3.09 \cdot 10^{-22}$ eV and $5 \cdot 10^{-22}$ eV with its initial position $r_0 = 1.5$ kpc in two cases with and without a damping term. The black horizontal line indicates the current position of GC3.

also for non-interacting (fuzzy) ULDM.

For $m \gtrsim 10^{-21}$ eV, the Thomas-Fermi regime of strongly repulsive self-interacting ULDM is realized. According to the results of Fig.5, one can see that the maximum time for GC3 to move from the initial position $r_0 = 1$ kpc from the center of the Fornax galaxy to its current position at $r_{GC3} = 0.64$ kpc is about 9 Gyr for the mass $m = 10^{-21}$ eV and decreases as the mass increases. Thus, in this case, we cannot provide a necessary infall time.

The role of the damping term ($\xi \neq 0$) is demonstrated in Fig.6 for two values of mass $m = 3.09 \cdot 10^{-22}$ eV and $5 \cdot 10^{-22}$ eV. Clearly, damping results in an increase of the infall time. Fixing the DM mass $m = 4 \cdot 10^{-22}$ eV and including the damping term, the trajectory $r(t)$ of the globular cluster GC3 as a function of time is plotted in Fig.7 for different initial positions in the range $1 \text{ kpc} < r_0 < 1.7 \text{ kpc}$. The black horizontal line indicates the current position of GC3. As expected, the infall time grows as the initial distance increases.

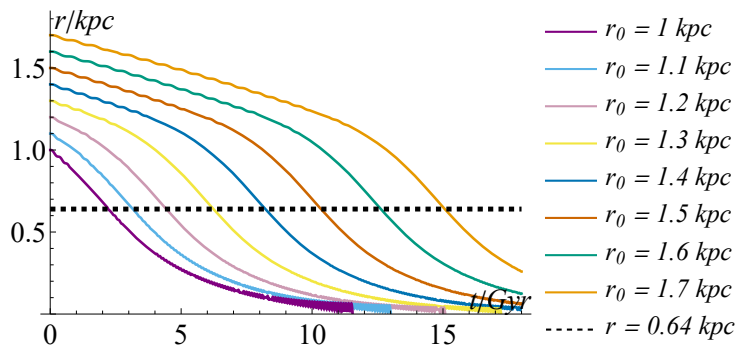


Figure 7: The trajectory $r(t)$ of the globular cluster GC3 as a function of time for the value of the ULDM boson mass $m = 4 \cdot 10^{-22}$ eV with its initial position in the range $1 \text{ kpc} < r_0 < 1.7 \text{ kpc}$. The black horizontal line indicates the current position of GC3.

7 Conclusions

In this work, we investigated the dynamical friction force acting on orbiting globular clusters in the Fornax dwarf galaxy. We modeled dark matter composed of ultralight bosons by the generalized Gross-Pitaevskii-Poisson equation and, in particular, studied the impact of the damping term. The case of the globular cluster GC3 is the most interesting and problematic because GC3 is considered to be formed in situ, has an estimated age of approximately 12 Gyr, and is located at present at a large distance of 0.64 kpc from the center of the Fornax dwarf galaxy.

We derived analytical expression for the dynamical friction force (16) acting on circularly moving point objects in ULDM models both with and without the damping term in the generalized Gross-Pitaevskii-Poisson equation (1). This force arises due to gravitational interaction with the ULDM density perturbation induced by the moving object.

In our numerical calculations, we considered only the case of repulsive self-interacting ULDM in the regimes of weak (Gaussian) and strong (Thomas-Fermi) self-interaction. We found that there is a lower bound of ULDM boson mass $m_{low} \approx 3.09 \cdot 10^{-22}$ eV. As one can see from the mass-radius relation (27), for smaller values of mass, the repulsive interaction turns into an attractive interaction.

Results of the computation of the dynamical friction force as a function of ULDM boson mass and distance from the center of Fornax dwarf galaxy are given in Fig.3 for the case with and without the damping term in the Gross-Pitaevskii equation. Our main finding is that the damping term essentially modifies (decreases) the magnitude of the dynamical friction force acting on stars, globular clusters, or dwarf galaxies moving in the ultralight dark matter halo. This decrease takes place because damping inhibits the ULDM density perturbation caused by moving objects.

For the globular cluster GC3, we calculated its dynamical trajectory and found the infall time from the initial point at distances $r_0 = 1$ kpc and $r_0 = 1.5$ kpc to the current position at $r_{GC3} = 0.64$ kpc from center of the Galaxy, see Fig.4 and Fig.5. According to our results, in the case of weakly self-interacting (the Gaussian regime) ULDM, the infall time of GC3 can attain the required value $T_{GC3} = 12$ Gyr for a ULDM boson mass $m \gtrsim m_{low}$, provided that ULDM is non-interacting or has a very small repulsive self-interaction. In the strongly-interacting ULDM (the Thomas-Fermi regime), there is no solution for the infall time be equal to T_{GC3} if the starting position is $r_0 \lesssim 1.5$ kpc.

To illustrate more clearly the impact of the damping term ($\xi \neq 0$), we plot the trajectory $r(t)$ of the globular cluster GC3 as a function of time in Fig.6 in two cases with and without a damping term. The inclusion of damping noticeably delays the orbital decay, leading to a significantly longer infall time compared to the case without damping.

To further explore this effect, we fix the dark matter mass at $m = 4 \cdot 10^{-22}$ eV and analyze the time evolution of the orbital radius $r(t)$ for the globular cluster GC3 as a function of initial distance. The corresponding trajectories are shown in Fig.7 for a range of initial positions $1 \text{ kpc} < r_0 < 1.7 \text{ kpc}$. As expected, clusters starting at larger radii require more time to reach the observed current position. For sufficiently large initial distances r_0 , the infall time can match the required values even for higher dark matter masses m . In this case, viable solutions are not restricted to the Gaussian regime but can also be realized within the Thomas-Fermi regime.

Acknowledgements

The authors are grateful to B.I. Hnatyk and A.I. Yakimenko for fruitful discussions and helpful comments. K.K. acknowledges funding by the Deutsche Forschungsgemeinschaft (DFG, German Research Foundation) under Germany's Excellence Strategy – EXC 2123 QuantumFrontiers – 390837967. The work of E.V.G., V.M.G., and A.O.Z. was partially supported by the project 'Search for dark matter and particles beyond the Standard Model' of the Ministry of Education and Science of Ukraine (25BF051-01).

Appendix

The motion of a globular cluster of mass m_{GC} in the gravitational field of the Fornax dwarf galaxy, subject, in addition, to the dynamical friction force due to perturbed ultralight dark matter, is governed by the equation

$$m_{\text{GC}}\ddot{\mathbf{r}} = \mathbf{F}_{\text{grav}} + \mathbf{F}_{\text{fr}}, \quad (\text{A.1})$$

where the dynamical friction force is given by Eq. (16) and the gravitational force equals

$$\mathbf{F}_{\text{grav}} = -\frac{Gm_{\text{GC}}M(r)}{r^2}\hat{\mathbf{r}}. \quad (\text{A.2})$$

Here, the enclosed mass of the Fornax galaxy within radius r is

$$M(r) = \int_0^r 4\pi\rho(r')r'^2 dr', \quad (\text{A.3})$$

where $\rho(r)$ is the ULDM density profile.

Decomposing the equation of motion (A.1) into the radial and azimuthal components ($\hat{\mathbf{r}}, \hat{\boldsymbol{\phi}}$), we find

$$m_{\text{GC}}(\ddot{r} - r\dot{\phi}^2)\hat{\mathbf{r}} + m_{\text{GC}}(r\ddot{\phi} + 2\dot{r}\dot{\phi})\hat{\boldsymbol{\phi}} = -\frac{Gm_{\text{GC}}M(r)}{r^2}\hat{\mathbf{r}} - F_r\hat{\mathbf{r}} - F_t\hat{\boldsymbol{\phi}}. \quad (\text{A.4})$$

Projecting this equation onto the radial and tangential directions gives

$$\begin{cases} m_{\text{GC}}(\ddot{r} - r\dot{\phi}^2) = -\frac{Gm_{\text{GC}}M(r)}{r^2} - F_r, \\ \frac{1}{r}\frac{d}{dt}(m_{\text{GC}}r^2\dot{\phi}) = -F_t. \end{cases} \quad (\text{A.5})$$

Introducing the angular momentum

$$l = m_{\text{GC}}r^2\dot{\phi}, \quad (\text{A.6})$$

the above equations can be rewritten in the form (47), where the term $F_r(t)$ is neglected because it is much smaller than the first term.

References

- [1] R. Gratton, A. Bragaglia, E. Carretta, V. D’Orazi, S. Lucatello and A. Sollima, *What is a globular cluster? an observational perspective*, *The Astronomy and Astrophysics Review* **27** (2019) 8.
- [2] S. Tremaine, J. Ostriker and S. Spitzer, *The formation of the nuclei of galaxies. I. M31.*, *The Astrophysical Journal* **196** (1975) 407.
- [3] A.B. Pace, M.G. Walker, S.E. Koposov, N. Caldwell, M. Mateo, E.W. Olszewski et al., *Spectroscopic confirmation of the sixth globular cluster in the Fornax dwarf spheroidal galaxy*, *The Astrophysical Journal* **923** (2021) 77.
- [4] S. Tremaine, *The formation of the nuclei of galaxies. II - The local group*, *The Astrophysical Journal* **203** (1976) 345.
- [5] K. Oh, D. Lin and H. Richer, *Globular clusters in the Fornax dwarf spheroidal galaxy*, *The Astrophysical Journal* **531** (2000) 727.
- [6] N. Meadows, J. Navarro, I. Santos-Santos, A. Benitez-Llambay and C. Frenk, *Cusp or core? Revisiting the globular cluster timing problem in Fornax*, *Mon. Not. Roy. Astron. Soc.* **491** (2020) 3336.
- [7] N. Bar, S. Danieli and K. Blum, *Dynamical friction in globular cluster-rich ultra-diffuse galaxies: The case of NGC5846-UDG1*, *The Astrophysical Journal Letters* **932** (2021) L10.
- [8] F. Sanchez-Salcedo, J. Reyes-Iturbide and X. Hernandez, *An extensive study of dynamical friction in dwarf galaxies: the role of stars, dark matter, halo profiles and MOND*, *Monthly Notices of the Royal Astronomical Society* **370** (2006) 1829.
- [9] D. Cole, W. Dehnen, J. Read and M. Wilkinson, *The mass distribution of the Fornax dSph: constraints from its globular cluster distribution*, *Monthly Notices of the Royal Astronomical Society* **426** (2012) 1829.
- [10] T. Goerdt, B. Moore, J. Read, J. Stadel and M. Zemp, *Does the Fornax dwarf spheroidal have a central cusp or core?*, *Monthly Notices of the Royal Astronomical Society* **368** (2006) 1073.
- [11] P. Boldrini, R. Mohayaee and J. Silk, *Fornax globular cluster distributions: implications for the cusp-core problem*, *Monthly Notices of the Royal Astronomical Society* **485** (2019) 2546.
- [12] E.G.M. Ferreira, *Ultra-light dark matter*, *Astron. Astrophys. Rev.* **29** (2021) 7 [2005.03254].
- [13] P.-H. Chavanis, *A review of basic results on the Bose–Einstein condensate dark matter model*, *Front. Astron. Space Sci.* **12** (2025) 1538434.
- [14] N. Bar, S. Danieli and K. Blum, *Dynamical friction in globular cluster-rich ultra-diffuse galaxies: the case of ngc5846-udg1*, *The Astrophysical Journal* **932** (2022) L10.

- [15] P.-H. Chavanis, *Predictive model of BEC dark matter halos with a solitonic core and an isothermal atmosphere*, *Physical Review D* **100** (2019) 083022.
- [16] H.-Y. Schive, M.-H. Liao, T.-P. Woo, S.-K. Wong, T. Chiueh, T. Broadhurst et al., *Understanding the Core-Halo Relation of Quantum Wave Dark Matter from 3D Simulations*, *Phys. Rev. Lett.* **113** (2014) 261302 [[1407.7762](#)].
- [17] L. Hui, J.P. Ostriker, S. Tremaine and E. Witten, *Ultralight scalars as cosmological dark matter*, *Phys. Rev. D* **95** (2017) 043541 [[1610.08297](#)].
- [18] L. Lancaster, C. Giovanetti, P. Mocz, Y. Kahn, M. Lisanti and D.N. Spergel, *Dynamical Friction in a Fuzzy Dark Matter Universe*, *JCAP* **01** (2020) 001 [[1909.06381](#)].
- [19] T.J.L. de Boer and M. Fraser, *Four and one more: The formation history and total mass of globular clusters in the Fornax dSph*, *Astronomy & Astrophysics* **590** (2016) A35 [[1510.05642](#)].
- [20] N. Bar, D. Blas, K. Blum and H. Kim, *Assessing the Fornax globular cluster timing problem in different models of dark matter*, *Phys. Rev. D* **104** (2021) 043021 [[2102.11522](#)].
- [21] V. Desjacques, A. Nusser and R. Buehler, *Analytic solution to the dynamical friction acting on circularly moving perturbers*, *The Astrophysical Journal* **928** (2022) 64.
- [22] R. Buehler and V. Desjacques, *Dynamical friction in fuzzy dark matter: Circular orbits*, *Phys. Rev. D* **107** (2023) 023516 [[2207.13740](#)].
- [23] V.M. Gorkavenko, A.I. Yakimenko, A.O. Zaporozhchenko and E.V. Gorbar, *Dynamical friction in ultralight dark matter: Plummer sphere perspective*, *Phys. Scripta* **100** (2025) 075039 [[2412.15428](#)].
- [24] O.V. Barabash, T.V. Gorkavenko, V.M. Gorkavenko, O.M. Teslyk, N.S. Yakovenko, A.O. Zaporozhchenko et al., *Analytic Calculation of Dynamical Friction for Plummer Sphere in Ultralight Dark Matter*, *Ukr. J. Phys.* **70** (2025) 759 [[2504.06448](#)].
- [25] L. Berezhiani, G. Cintia, V. De Luca and J. Khoury, *Dynamical friction in dark matter superfluids: The evolution of black hole binaries*, *JCAP* **06** (2024) 024 [[2311.07672](#)].
- [26] J.R. Jardel and K. Gebhardt, *The dark matter density profile of the Fornax dwarf*, *The Astrophysical Journal* **746** (2012) 89.
- [27] A.W. McConnachie, *The observed properties of dwarf galaxies in and around the local group*, *The Astronomical Journal* **144** (2012) 4.
- [28] P.-H. Chavanis, *Mass-radius relation of Newtonian self-gravitating Bose-Einstein condensates with short-range interactions: I. Analytical results*, *Phys. Rev. D* **84** (2011) 043531 [[1103.2050](#)].

- [29] P.-H. Chavanis, *Self-gravitating Bose-Einstein condensates*, *Quantum Aspects of Black Holes* (2015) 151.
- [30] P.-H. Chavanis, *Derivation of the core mass – halo mass relation of fermionic and bosonic dark matter halos from an effective thermodynamical model*, *Phys. Rev. D* **100** (2019) 123506 [[1905.08137](#)].
- [31] P.-H. Chavanis, *Jeans mass-radius relation of self-gravitating Bose-Einstein condensates and typical parameters of the dark matter particle*, *Phys. Rev. D* **103** (2021) 123551 [[2011.01038](#)].
- [32] P.-H. Chavanis, *Mass-radius relation of self-gravitating Bose-Einstein condensates with a central black hole*, *The European Physical Journal Plus* **134** (2019) 352.
- [33] J.F. Navarro, C.S. Frenk and S.D.M. White, *A Universal density profile from hierarchical clustering*, *Astrophys. J.* **490** (1997) 493 [[astro-ph/9611107](#)].
- [34] J. Binney and S. Tremaine, *Galactic dynamics*, vol. 13, Princeton university press (2011).
- [35] M.G. Walker, M. Mateo, E.W. Olszewski, O.Y. Gnedin, X. Wang, B. Sen et al., *Velocity Dispersion Profiles of Seven Dwarf Spheroidal Galaxies*, *Astrophys. J. Lett.* **667** (2007) L53 [[0708.0010](#)].